Virology 436 (2013) 173–178

Contents lists available at SciVerse ScienceDirect

Virology

journal homepage: www.elsevier.com/locate/yviro

A common structure for the potexviruses

Amy Kendall [a], Wen Bian [a], Alexander Maris [a], Caitlin Azzo [a], Joseph Groom [a,1], Dewight Williams [b,2], Jian Shi [b,3], Phoebe L. Stewart [b,4], Joseph S. Wall [c], Gerald Stubbs [a,*]

[a] Department of Biological Sciences and Center for Structural Biology, Vanderbilt University, Nashville, TN 37235, USA
[b] Department of Molecular Physiology and Biophysics and Center for Structural Biology, Vanderbilt University, Nashville, TN 37232, USA
[c] Biology Department, Brookhaven National Laboratory, Upton, NY 11973, USA

ARTICLE INFO

Article history:
Received 14 September 2012
Returned to author for revisions
15 October 2012
Accepted 12 November 2012
Available online 11 December 2012

Keywords:
Potexvirus
Potato virus X
Papaya mosaic virus
Narcissus mosaic virus
Helical symmetry
Fiber diffraction
Cryo-electron microscopy
STEM

ABSTRACT

We have used fiber diffraction, cryo-electron microscopy, and scanning transmission electron microscopy to confirm the symmetry of three potexviruses, potato virus X, papaya mosaic virus, and narcissus mosaic virus, and to determine their low-resolution structures. All three viruses have slightly less than nine subunits per turn of the viral helix. Our data strongly support the view that all potexviruses have approximately the same symmetry. The structures are dominated by a large domain at high radius in the virion, with a smaller domain, which includes the putative RNA-binding site, extending to low radius.

Introduction

The potexviruses – flexible filamentous plant viruses belonging to the family *Alphaflexiviridae* – were early candidates for structural studies (Bernal and Fankuchen, 1941). Electron microscopy and diffraction studies have described a number of different potexviruses, including potato virus X (PVX; Tollin et al., 1980), narcissus mosaic virus (NMV; Tollin et al., 1975; Bancroft et al., 1980; Low et al., 1985), and papaya mosaic virus (PapMV; Tollin et al., 1979). The gross architecture of all members of the potexvirus group is thought to be very similar (Richardson et al., 1981). More recent fiber diffraction studies (Parker et al., 2002) and combined fiber diffraction and electron microscopy studies (Kendall et al., 2008) of the potexviruses have supported these conclusions.

Over the years, however, symmetries inconsistent with these results have occasionally been reported for members of the potexvirus group (Tollin et al., 1975; Wilson et al., 1978; Radwan et al., 1981; Kendall et al., 2007). Even very recently, a low-resolution potexvirus model in disagreement with the now generally accepted symmetry of these viruses has been published (Yang et al., 2012).

Cryo-electron microscopy (cryoEM) has increasingly been used in the determination of the structures of filamentous assemblies that are otherwise not amenable to crystallographic, fiber diffraction, or nuclear magnetic resonance studies. Helical image processing methods such as iterative helical real-space reconstruction (IHRSR; Egelman, 2010) can produce low- to medium-resolution models of these assemblies; however, most models derived by helical image processing methods are at low resolution, rarely going beyond 10 Å. Models of the well-studied and highly ordered tobacco mosaic virus (TMV), whose structure was determined at 2.9 Å resolution by fiber diffraction (Namba et al., 1989), are exceptions (Sachse et al., 2007; Clare and Orlova, 2010; Ge and Zhou, 2011), as are those of a few other assemblies (for example, Fujii et al., 2010; Yu et al., 2012). Because it is necessary to have a reasonable estimate of the symmetry of a filamentous model before beginning IHRSR experiments (Egelman, 2007), helical reconstructions frequently use

* Corresponding author. Fax: +615 343 6707.
E-mail address: gerald.stubbs@vanderbilt.edu (G. Stubbs).
[1] Current address: Department of Genetics, University of Georgia, Athens, GA 30602, USA
[2] Current address: Electron Microscopy Resource Laboratory, University of Pennsylvania, Philadelphia, PA 19104, USA
[3] Current address: Centre for BioImaging Sciences, National University of Singapore, Singapore
[4] Current address: Department of Pharmacology and Cleveland Center for Membrane and Structural Biology, Case Western Reserve University, Cleveland, OH 44106, USA

0042-6822/$ - see front matter © 2012 Elsevier Inc. All rights reserved.
http://dx.doi.org/10.1016/j.virol.2012.11.008

information from other techniques such as crystallography or scanning transmission electron microscopy (STEM) to guide modeling; in fact, these additional methods are frequently necessary to resolve ambiguities in symmetry determination (Egelman, 2010; Yu and Egelman, 2010). Fiber diffraction can provide constraints to guide helical reconstructions (Wang et al., 2006; Kendall et al., 2008), limiting the possible solutions.

We report here low-resolution models of two potexviruses, PapMV and NMV, and compare them to PVX, for which we have already described a low-resolution model (Kendall et al., 2008). The three models share a similar architecture and symmetries of slightly less than nine coat protein subunits per turn of the viral helix.

Results

Data collected from fiber diffraction and STEM experiments were used to constrain helical reconstruction.

Fiber diffraction

Fig. 1 is an X-ray diffraction pattern from a hydrated fiber of PapMV (Materials and methods; McDonald et al., 2008). The pitch of the PapMV viral helix determined from this pattern is 33.7 ± 0.3 Å, in good agreement with early diffraction studies (Tollin et al., 1979).

The pattern consists of strong near-meridional layer lines (black arrows in Fig. 1), whose spacing reflects the helical pitch, and weaker off-meridional lines. If the number of subunits per turn is $u = u_i + \Delta u$, where u_i is an integer and Δu is between -0.5 and 0.5, Δu can be determined from the distance between the near-meridional and off-meridional layer lines. Δu is equal to the ratio of Δz, the spacing between a near-meridional layer line and its nearest neighboring off-meridional layer line, and $1/p$, the spacing between near-meridional layer lines, that is, $\Delta u = \pm p\,\Delta z$, where p is the pitch of the viral helix (Cochran et al., 1952; Chandrasekaran and Stubbs, 2012; McDonald et al., 2010). From the positions of the 14th and 19th layer lines (layer lines $3(-1)$ and $4(-1)$ in the notation of McDonald et al., 2010; white arrows in Fig. 1), Δu is ± 0.2, with an estimated error of ± 0.04.

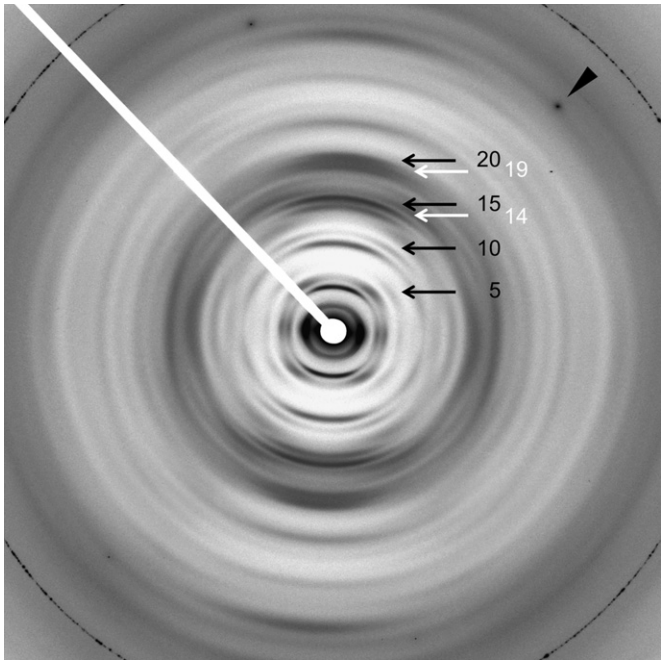

Fig. 1. Fiber diffraction pattern from a hydrated fiber of PapMV. The pattern consists of layer lines (approximately horizontal in this figure); the layer line passing through the origin is the equator. The line through the origin orthogonal to the equator is the meridian. Black arrows and numbers indicate near-meridional layer lines, layer lines whose intensities are significant at or near the meridian. The spacing of these layer lines corresponds to the reciprocal of the pitch. White arrows and numbers indicate off-meridional (non-near-meridional) layer lines, whose positions relative to the near-meridional layer lines allow the determination of the non-integral part of the number of subunits in one turn of the viral helix. Strong reflections at 4–5 Å resolution (arrowhead and its three symmetry equivalents) are from the mica entry window of the beam tunnel; the ring of reflections in the corners of the pattern at 3.85 Å resolution is from calcite, used for calibration. The diagonal white shadow is from the beamstop holder.

The sign of Δu can often be determined directly by examination of the fiber diffraction pattern; in the present case, the 14th and 19th layer lines have intensity maxima near the meridian, indicating that Δu is -0.2. If Δu were $+0.2$, the 16th and 21st layer lines, rather than the 14th and 19th, would have maxima near the meridian (Kendall et al., 2008).

The helical pitches of PVX (34.5 ± 0.5 Å; Parker et al., 2002) and NMV (34.5 ± 0.5 Å; Kendall et al., 2007) have previously been determined by fiber diffraction.

STEM

Additional constraints to guide the helical reconstructions were provided by STEM. The predicted molecular mass of one intact protein subunit of PapMV is 23,045 Da (GenPept accession no. BAA03054). The RNA sequence length (GenBank accession no. NC_001748), the length of the virion, and a preliminary estimate of the helical symmetry suggest that each PapMV protein subunit binds five nucleotides. For STEM analysis, the mass of one subunit was taken to be 24650 (23045 plus five nucleotides with an average molecular mass of 321 Da). Two separate STEM experiments were performed, using data from the same grid collected on the same day. The first experiment used 1625 PapMV particles and determined the mass per unit length to be 6002 ± 414 Da/Å. The second experiment contained 1376 PapMV particles and determined the mass per unit length to be 6051 ± 514 Da/Å. From these values, the subunit mass, and the helical pitch of 33.7 Å, u was determined to be 8.21 ± 0.57 from the first set of particles and 8.27 ± 0.71 from the second set. These estimates of u are probably low because of the effect of protein degradation on the average subunit mass; PapMV coat protein is known to be sensitive to N-terminal proteolysis (Verde et al., 1989; Zhang et al., 1993). SDS-PAGE analysis similar to that of Kendall et al. (2008) suggested that the underestimation of u due to proteolytic degradation was less than 2%.

IHRSR

PapMV IHRSR experiments (Fig. 2A) were started from symmetries ranging from 7.5 to 11.6 subunits per turn of the helix, extending well beyond the range of values predicted by STEM. Reconstructions started between 8.67 and 8.82 subunits per turn all converged to a symmetry of 8.76 subunits per turn (Fig. 2A) with a helical pitch of 33.4 Å, within experimental error of the fiber diffraction pitch. Experiments started outside this range produced models that deviated from the fiber diffraction pitch, the sign of Δu from fiber diffraction, or both, and in many cases deviated significantly from the mass per unit length determined by STEM. None of the models with the sign of Δu determined by fiber diffraction were within four times the experimental error of the fiber diffraction pitch except those with 8.76 subunits per turn. Models with more than 9.5 subunits per turn all had pitches 3–5 times the true pitch.

NMV IHRSR experiments (Fig. 2B) were started from symmetries ranging from 7.5 to 9.2 subunits per turn. Reconstructions

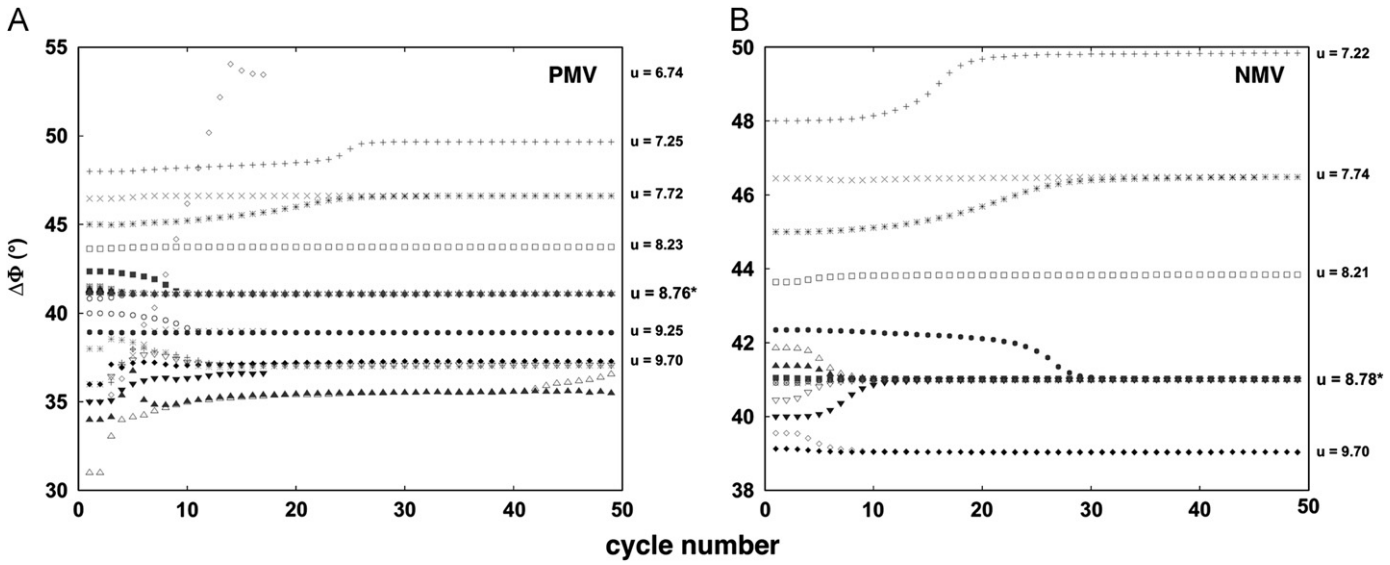

Fig. 2. (A) Convergence of the rotation angle $\Delta\Phi$ in PapMV IHRSR experiments. Reconstructions started between $\Delta\Phi=40.82^\circ$ and $\Delta\Phi=41.52^\circ$ ($u=8.67$–8.82) converged to a symmetry of $u=8.76$ and a helical pitch of 33.4 Å (*); experiments started outside this range produced models that conflicted with fiber diffraction and STEM results. The reconstructions started at $\Delta\Phi=31^\circ$ and $\Delta\Phi=34^\circ$ converged to $u=9.70$ by cycle 70. (B) Convergence of the rotation angle $\Delta\Phi$ in NMV IHRSR experiments. Experiments started between $\Delta\Phi=40.00$ and $\Delta\Phi=42.35$ degrees ($u=8.5$–9.0) converged to a symmetry of $u=8.78$ and a helical pitch of 34.5 Å (*); experiments started outside this range produced models that conflicted with fiber diffraction results.

started between 8.5 and 9.0 subunits per turn all converged to a symmetry of 8.78 subunits per turn (Fig. 2B) with a helical pitch of 34.5 Å. Reconstructions started outside these values produced models incompatible with the pitch determined by fiber diffraction.

PVX IHRSR experiments were started from a symmetry of 8.9 subunits per turn (Kendall et al., 2008) and converged to 8.89 subunits per turn with a helical pitch of 34.9 Å. The models were similar in all essential details to the models described in our earlier work.

The nominal resolution for each of these models, determined using the routines available in the IHRSR script (Materials and methods), was 21 Å for PVX, 16 Å for NMV, and 16 Å for PapMV. When virus particle images were first separated into two stacks with approximately equal numbers of particles and similar ranges of defocus values (Yamaguchi et al., 2010), and models were calculated independently, aligned, and correlated to each other, the nominal resolution for each model was between 20 and 22 Å.

Refined models of PVX, NMV, and PapMV are shown in Fig. 3. For these reconstructions, the starting and final symmetries were 8.90 and 8.89 subunits per turn (PVX), 8.77 and 8.78 subunits per turn (NMV), and 8.77 and 8.74 subunits per turn (PapMV); the starting and final pitches were 34.51 and 34.90 Å (PVX), 34.47 and 34.56 Å (NMV), and 33.39 and 33.40 Å (PapMV). The maximum radius of both PVX and NMV (Fig. 3A and B) is approximately 65 Å, while the maximum radius of PapMV (Fig. 3C) is approximately 60 Å. PapMV has a smaller radius because the ridges between the approximately vertical grooves in the virion surface are less extensive; that is, the grooves are shallower than they are in PVX and NMV. In all three viruses, the protein subunit structure is dominated by a major domain at high radius with density extending into the virion center, as previously seen for PVX and the potyvirus soybean mosaic virus (Kendall et al., 2008). Axial intersubunit interactions are greater at high radii, and azimuthal interactions at low radii.

The viral RNA is expected to be at a radius of 30 to 35 Å (Kendall et al., 2007, 2008). If this is the case, density in all three viruses (arrows in Fig. 3) at about this radius and extending across several subunits may represent the RNA, although at this resolution such a speculation should be treated with caution.

At low radii, the subunits in the vertical cross-sections in Fig. 3 exhibit a double-layered appearance, reminiscent of the structure of TMV (Namba et al., 1989). However, given the low resolution of these reconstructions, we cannot speculate about the possible presence of an α-helical bundle such as is found in the TMV coat protein.

Discussion

The three potexvirus structures determined here are all very similar to each other and to the previously determined structure of PVX (Kendall et al., 2008). The most obvious difference is the smaller diameter of PapMV, about 120 Å compared with 130 Å for both PVX and NMV. The helical pitch of PapMV is also slightly smaller than those of PVX and NMV. These differences are consistent with the smaller size of the PapMV coat protein, 215 amino acids (GenPept accession number BAA03054) compared with 237 (PVX; GenPept accession number P31798) and 240 (NMV; GenPept accession number BAA02895).

The overall subunit structure that we have described here is broadly consistent with the two-domain model of Nemykh et al. (2008) predicted from sequence and other considerations. The larger predominantly α-helical domain would correspond to the large high-radius domain that we see in all three viruses, while the smaller domain, which resembles the four-helix bundle seen in TMV, could correspond to our low-radius double-layered domain. The crystal structure of a large fragment of PapMV coat protein (Yang et al., 2012) also resembles our high-radius domain. However, the helical symmetry suggested for PapMV by Yang et al. (2012), 10.25 subunits per turn, is very different from the symmetry that we have determined, and is inconsistent with our cryo-EM reconstructions, our STEM data, and our fiber diffraction data.

PapMV, PVX, and NMV coat proteins are very similar in amino acid sequence, with coat protein sequence identities of 39% (PVX:PapMV), 35% (PVX:NMV) and 30% (PapMV:NMV); similarities of 68% (PVX:PapMV), 62% (PVX:NMV) and 59% (PapMV:NMV). It would therefore be extremely surprising if their helical symmetries were greatly different, and our data suggest

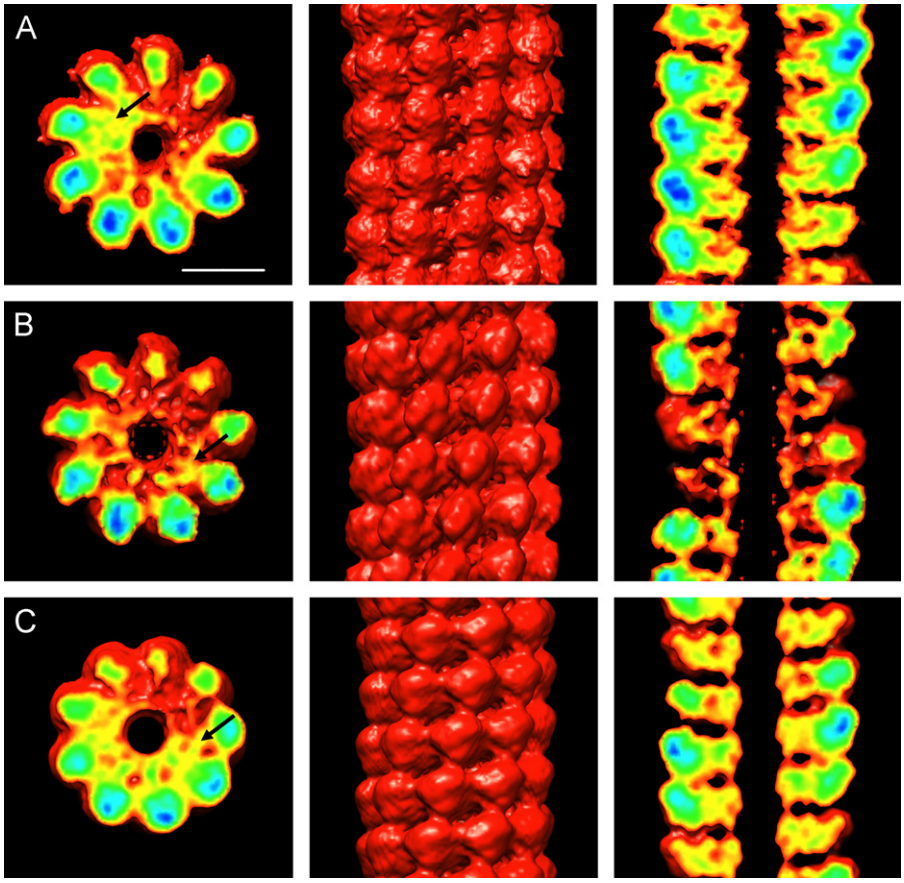

Fig. 3. IHRSR models of potexviruses. (A) IHRSR reconstruction of PVX, section normal to the viral axis, outside surface view, and section through the viral axis. Scale bar=50 Å and applies to all panels. (B) IHRSR reconstruction of NMV, section normal to the viral axis, outside surface view, and section through the viral axis. (C) IHRSR reconstruction of PapMV, section normal to the viral axis, outside surface view, and section through the viral axis. Arrows in sections normal to the viral axis indicate possible RNA density.

that they are in fact very similar. The apparent differences suggested by Yang et al. (2012) may be due to the fact that they did not start refinements close to the symmetries proposed in previous work, and did not use restraints on symmetries from other methods such as STEM or fiber diffraction. Both of these strategies have been found to be necessary in IHRSR (Egelman, 2007, 2010; Yu and Egelman, 2010). The 36 Å pitch reported by Yang et al. (2012) is significantly greater than the 33.7 Å pitch from fiber diffraction.

Materials and methods

Virus purification

Potato virus X was propagated in *Nicotiana clevelandii* and purified as described by Parker et al. (2002). Narcissus mosaic virus was propagated in *Chenopodium quinoa* and purified as described by Kendall et al. (2007). Papaya mosaic virus was propagated in *Carica papaya* var. Mexican and purified using a protocol adapted from that of Erickson and Bancroft (1978), incorporating the use of protease inhibitors.

Fiber diffraction

Dried fibers of PapMV were prepared by suspending a 5 µl drop of virus solution at a concentration of approximately 50 mg/ml between two glass rods approximately 1 mm apart, and allowing the drop to dry over a period of hours to days. Humidity control was essential during drying; the fibers were made in closed chambers in the presence of water, to produce a relative humidity close to 100% (McDonald et al., 2008).

Fiber diffraction data were collected at beamline 4–2 of the Stanford Synchrotron Radiation Lightsource. Fibers were dusted with calcite, and wide-angle specimen-to-detector distances were determined from the 0 1 2 calcite diffraction ring at 3.8547 Å resolution (Effenberger et al., 1981). The specimen-to-detector distance was approximately 323 mm, the pixel size was approximately 73 µm, and the X-ray wavelength was 1.078 Å.

Diffraction patterns were analyzed using the program WCEN (Bian et al., 2006) to determine experimental parameters and the helical repeat, to apply corrections to the intensities, and to transform the data from detector to reciprocal space.

STEM

Scanning transmission electron microscopy (Wall et al., 2008) was used to determine the mass per unit length of the PapMV virions. Images were analyzed using the PCMass software available from the Brookhaven STEM website (www.biology.bnl.gov/stem/stem.html). Mass per unit length measurements were calibrated against measurements from a TMV internal standard.

Electron microscopy, helical reconstruction, and image processing

PVX and NMV at concentrations of ~100 µg/ml were applied to freshly glow discharged carbon coated 400 square mesh copper EM grids (Electron Microscopy Sciences, Hatfield, PA). Excess

liquid was blotted away with filter paper and the grid was plunged into liquid nitrogen cooled ethane using a homemade vitrification device. Images were collected on an FEI TF30 Polara microscope at 300 keV, 78 K, with a magnification of 254,669 at the level of the Gatan US4000 CCD camera. The total electron dose varied between 10 and 25 electron/Å^2. Imaging was facilitated by the script assisted microscopy package (Shi et al., 2008). Digital images were software binned to 1.178 Å/pixel (PVX) or 2.356 Å/pixel (NMV) and normalized to 10σ of the mean pixel value.

Cryo-EM grids of PapMV were prepared by applying 3 μl of sample to 2/2 C-flat grids (ProtoChips Inc., Raleigh, NC) and vitrified as described in the previous paragraph. Cryo-EM images were collected on an FEI Tecnai 12 (120 keV) electron microscope equipped with a Gatan cryo holder and a Gatan UltraScan 1000 (2 K × 2 K) CCD camera at a nominal magnification of 67,000 (1.47 Å/pixel). Images were normalized to 10σ of the mean pixel value.

The defocus values of the micrographs were determined using CTFFIND3 (Mindell and Grigorieff, 1993) or CTFIT from the EMAN suite (Ludtke et al., 1999). Nine hundred fifty-three micrographs were collected from PVX grids; defocus values for these micrographs varied from 1.1 to 3.3 μm. Seventeen micrographs were collected from NMV grids; defocus values varied from 0.9 to 2.9 μm. Twenty eight micrographs were collected from PapMV grids; defocus values varied from 0.7 to 1.5 μm. These values were used to correct for the phase component of the contrast transfer function using scripts from the IHRSR++ package (Parent et al., 2010).

Virion segments were selected using the program HELIXBOXER from the EMAN suite (Ludtke et al., 1999); only straight segments in which the helical repeat was clearly visible were selected. Approximately 18,000 segments were selected from PVX micrographs, approximately 9600 segments were selected from NMV micrographs, and approximately 9800 segments were selected from PapMV micrographs. Additional scripts from the IHRSR++ package were used to invert the density of the virus segments, to cut the segments into 200 × 400 pixel boxes, and to pad the boxes to 410 × 410 pixels. Reconstruction experiments used either IHRSR (Egelman, 2010) or IHRSR++ (Parent et al., 2010), both of which make use of the SPIDER software package (Frank et al., 1996). All reconstructed volumes were constrained to have inner radii of 10 Å and outer radii of 70 Å.

The resolution of each reconstructed model was determined by separating the segments into two stacks, one with the even numbered segments and one with the odd numbered segments, following the standard procedure in the IHRSR method (Egelman, 2010). Independent models were produced from each stack and correlated with each other. The resolution was determined by Fourier shell correlation (FSC; Harauz and van Heel, 1986), using a threshold value of 0.5. It has recently been suggested (Yu et al., 2012), however, that this approach can yield overly optimistic determinations of resolution, so a second approach to resolution determination was also used. The intact virus particle images were first divided into two stacks with equal representations of defocus values and then segmented into individual particles using the *helix_cutstk* script in IHRSR++ (Parent et al., 2010), to produce two stacks with approximately equal numbers of segments and similar ranges of defocus values (Yamaguchi et al., 2010). Models were independently produced from each stack, aligned with each other, and correlated using an FSC threshold of 0.5. UCSF Chimera (Pettersen et al., 2004) was used to generate models and density maps; threshold values for model contouring were set at 1σ.

Sequence comparisons

Sequence comparisons between the viral coat proteins were made using the default parameters in Clustal Omega (Sievers et al., 2011). Only the cores of the proteins were compared (PapMV: residues 3–207; NMV: 15–223; PVX: 20–229); the very short terminal extensions, whose presence or absence and sequence when present varies considerably within the genus, were omitted.

Acknowledgments

We thank Kristin Parent for discussions and advice, Michele McDonald and Beth Lin for help with sample preparation, and William Wan and Robert Kim for help with data collection. This work was supported by NSF grant MCB-0743931. Data analysis software was obtained from FiberNet (www.fiberdiffraction.org). Helical reconstruction in part used the resources of the Advanced Computing Center for Research and Education at Vanderbilt University. STEM at Brookhaven National Laboratory is supported in part by the U.S. Department of Energy Office of Biological and Environmental Research. Stanford Synchrotron Radiation Laboratory is a national user facility operated by Stanford University on behalf of the DOE. The SSRL Structural Molecular Biology Program is supported by the DOE Office of Biological and Environmental Research, and by the National Institutes of Health, National Institute of General Medical Sciences (including P41GM103393) and the National Center for Research Resources (P41RR001209). The contents of this publication are solely the responsibility of the authors and do not necessarily represent the official views of NIGMS, NCRR or NIH.

References

Bancroft, J.B., Hills, G.J., Richardson, J.F., 1980. A re-evaluation of the structure of narcissus mosaic virus and polymers made from its protein. J. Gen. Virol. 50, 451–454.

Bernal, J.D., Fankuchen, I., 1941. X-ray and crystallographic studies of plant virus preparations. J. Gen. Physiol. 28, 111–165.

Bian, W., Wang, H., McCullough, I., Stubbs, G., 2006. WCEN: a computer program for initial processing of fiber diffraction patterns. J. Appl. Crystallogr. 39, 752–756.

Chandrasekaran, R., Stubbs, G., 2012. Fibre diffraction. In: Arnold, E., Himmel, D.M., Rossman, M.G. (Eds.), International Tables for Crystallography, Volume F: Crystallography of Biological Macromolecules, second ed. Wiley, Chichester, UK, pp. 583–592.

Clare, C.D., Orlova, E.V., 2010. 4.6 Å cryo-EM reconstruction of tobacco mosaic virus from images recorded at 300 keV on a 4 K × 4 K CCD camera. J. Struct. Biol. 171, 303–308.

Cochran, W., Crick, F.H.C., Vand, V., 1952. The structure of synthetic polypeptides. I. The transform of the atoms on a helix. Acta Crystallogr. 5, 581–586.

Effenberger, H., Mereiter, K., Zemann, J., 1981. Crystal structure refinement of magnesite, calcite, rhodochrosite, siderite, smithonite, and dolomite, with discussion of some aspects of the stereochemistry of calcite type carbonates. Z. Kristallogr. 156, 233–243.

Egelman, E.H., 2007. The iterative helical real space reconstruction method: surmounting the problems posed by real polymers. J. Struct. Biol. 157, 83–94.

Egelman, E.H., 2010. Reconstruction of helical filaments and tubes. Methods Enzymol. 482, 167–183.

Erickson, J.W., Bancroft, J.B., 1978. The self-assembly of papaya mosaic virus. Virology 90, 36–46.

Frank, J., Radermacher, M., Penczek, P., Zhu, J., Li, Y., Ladjadj, M., Leith., A., 1996. *SPIDER* and *WEB*: processing and visualization of images in 3D electron microscopy and related fields. J. Struct. Biol. 116, 190–199.

Fujii, T., Iwane, A., Yanagida, T., Namba, K., 2010. Direct visualization of secondary structures of F-actin by electron cryomicroscopy. Nature 467, 724–729.

Ge, P., Zhou, Z.H., 2011. Hydrogen-bonding networks and RNA bases revealed by cryo electron microscopy suggest a triggering mechanism for calcium switches. Proc. Nat. Acad. Sci. U.S.A 108, 9627–9642.

Harauz, G., van Heel, M., 1986. Exact filters for general geometry three dimensional reconstruction. Optik 73, 146–156.

Kendall, A., Bian, W., Junn, J., McCullough, I., Gore, D., Stubbs, G., 2007. Radial density distribution and symmetry of a *Potexvirus*, narcissus mosaic virus. Virology 357, 158–164.

Kendall, A., McDonald, M., Bian, W., Bowles, T., Baumgarten, S.C., Shi, J., Stewart, P.L., Bullitt, E., Gore, D., Irving, T.C., Havens, W.M., Ghabrial, S.A., Wall, J.S., Stubbs, G., 2008. Structure of flexible filamentous plant viruses. J. Virol. 82, 9546–9554.

Low, J.N., Tollin, P., Wilson, H.R., 1985. The number of protein subunits per helix turn in narcissus mosaic virus particles. J. Gen. Virol. 66, 177–179.

Ludtke, S.J., Baldwin, P.R., Chiu, W., 1999. *EMAN*: semiautomated software for high-resolution single-particle reconstructions. J. Struct. Biol. 128, 82–97.
McDonald, M., Kendall, A., Bian, W., McCullough, I., Havens, W.M., Ghabrial, S.A., Stubbs, G., 2010. The architecture of the potyviruses. Virology 405, 309–313.
McDonald, M., Kendall, A., Tanaka, M., Weissman, J.S., Stubbs, G., 2008. Enclosed chambers for humidity control and sample containment in fiber diffraction. J. Appl. Crystallogr. 41, 206–209.
Mindell, J.A., Grigorieff, N., 1993. Accurate determination of local defocus and specimen tilt in electron microscopy. J. Struct. Biol. 142, 334–347.
Namba, K., Pattanayek, R., Stubbs, G., 1989. Visualization of protein-nucleic acid interactions in a virus; refinement on intact tobacco mosaic virus structure at 2.9 Å resolution by X-ray fiber diffraction. J. Mol. Biol. 208, 307–325.
Nemykh, M.A., Efimov, A.V., Novikov, V.K., Orlov, V.N., Arutyunyan, A.M., Dracher, V.A., Lukashina, E.V., Baratova, L.A., Dobrov, E.N., 2008. One more probable structural transition in potato virus X virions and a revised model of the virus coat protein structure. Virology 372, 61–71.
Parent, K., Sinkovits, R.S., Suhanovsky, M.M., Teschke, C.M., Egelman, E.H., Baker, T.S., 2010. Cryo-reconstructions of P22 polyheads suggest that phage assembly is nucleated by trimeric interactions among coat proteins. Phys. Biol. 7, 045004.
Parker, L., Kendall, A., Stubbs, G., 2002. Surface features of potato virus X from fiber diffraction. Virology 300, 291–295.
Pettersen, E.F., Goddard, T.D., Huang, C.C., Couch, G.S., Greenblatt, D.M., Meng, E.C., Ferrin, T.E., 2004. UCSF Chimera—a visualization system for exploratory research and analysis. J. Comput. Chem. 15, 1605–1612.
Radwan, M.M., Wilson, H.R., Duncan, G.H., 1981. Diffraction studies of tulip virus X particles. J. Gen. Virol. 56, 297–302.
Richardson, J.F., Tollin, P., Bancroft, J.B., 1981. The architecture of the potexviruses. Virology 112, 34–39.
Sachse, C., Chen, J.Z., Coureux, P.D., Stroupe, M.E., Fändrich, M., Grigorieff, N., 2007. High-resolution electron microscopy of helical specimens: a fresh look at tobacco mosaic virus. J. Mol. Biol. 371, 812–835.
Shi, J., Williams, D.R., Stewart, P.L., 2008. A script-assisted microscopy (SAM) package to improve data acquisition rates on FEI Tecnai electron microscopes equipped with Gatan CCD cameras. J. Struct. Biol 164, 166–169.
Sievers, F., Wilm, A., Dineen, D., Gibson, T., Karplus, K., Li, W., Lopez, R., McWilliams, H., Remmert, M., Söding, J., Thompson, J., Higgins, D., 2011. Fast, scalable generation of high-quality protein multiple sequence alignments using Clustal Omega. Mol. Syst. Biol. 7, 539, http://dx.doi.org/10.1038/msb.2011.75.
Tollin, P., Bancroft, J.B., Richardson, J.F., Payne, N.C., Beveridge, T.J., 1979. Diffraction studies of papaya mosaic virus. Virology 98, 108–115.
Tollin, P., Wilson, H.R., Bancroft, J.B., 1980. Further observations on the structure of particles of potato virus X. J. Gen. Virol. 49, 407–410.
Tollin, P., Wilson, H.R., Mowat, W.P., 1975. Optical diffraction from particles of narcissus mosaic virus. J. Gen. Virol. 29, 331–333.
Verde, C., Malorni, A., Parente, A., 1989. The primary structure of papaya mosaic coat protein: a revision. J. Protein Chem. 8, 795–805.
Wall, J.S., Simon, M.N., Lin, B.Y., Vinogradov, S.N., 2008. Mass mapping of large globin complexes by scanning transmission electron microscopy. Methods Enzymol. 436, 487–501.
Wang, Y.A., Yu, X., Overman, S., Tsuboi, M., Thomas, G.J., Egelman, E.H., 2006. The structure of a filamentous bacteriophage. J. Mol. Biol. 361, 209–215.
Wilson, H.R., Al-Mukhtar, J., Tollin, P., Hutcheson, A., 1978. Observations on the structure of particles of white clover mosaic virus. J. Gen. Virol. 39, 361–364.
Yamaguchi, T., Fujii, T., Abe, Y., Hirai, T., Kang, D., Namba, K., Hamasaki, N., Mitsuoka, K., 2010. Helical image reconstruction of the outward-open human erythrocyte band 3 membrane domain in tubular crystals. J. Struct. Biol. 169, 406–412.
Yang, S., Wang, T., Bohon, J., Laliberté Gagné, M.-È., Bolduc, M., Leclerc, D., Li, H., 2012. Crystal structure of the coat protein of the flexible filamentous papaya mosaic virus. J. Mol. Biol. 422, 263–273.
Yu, X., Egelman, E.H., 2010. Helical filaments of human Dmc1 protein on single-stranded DNA: a cautionary tale. J. Mol. Biol. 401, 544–551.
Yu, X., Goforth, C., Meyer, C., Rachel, R., Wirth, R., Schröder, G., Egelman, E., 2012. Filaments from *Ignicoccus hospitalis* show diversity of packing in proteins containing N-terminal type IV pilin helices. J. Mol. Biol. 422, 274–281.
Zhang, H., Todderud, E., Stubbs, G., 1993. Crystallization and preliminary x-ray analysis of papaya mosaic virus coat protein. J. Mol. Biol. 234, 885–887.